Designed beta-hairpins inhibit LDH5 oligomerization and enzymatic activity

Journal:	*Journal of Medicinal Chemistry*
Manuscript ID	jm-2020-018987.R2
Manuscript Type:	Article
Date Submitted by the Author:	16-Mar-2021
Complete List of Authors:	Nadal-Bufi, Ferran; Queensland University of Technology, School of Biomedical Sciences Mason, Jody; University of Bath, Department of Biology and Biochemistry Chan, Lai Yue; The University of Queensland, Institute for Molecular Bioscience Craik, David; University of Queensland, Institute for Molecular Bioscience Kaas, Quentin; University of Queensland, Institute for Molecular Bioscience Troeira Henriques, Sónia; Queensland University of Technology, School of Biomedical Sciences

Designed beta-hairpins inhibit LDH5 oligomerization and enzymatic activity

Ferran Nadal-Bufi[1], Jody M. Mason[2], Lai Yue Chan[3], David J. Craik[3], Quentin Kaas[3], and Sónia Troeira Henriques[1,3,*]

[1]Queensland University of Technology, School of Biomedical Sciences, Translational Research Institute, Brisbane, Queensland 4102, Australia

[2]Department of Biology and Biochemistry, University of Bath, Bath BA2 7AY, United Kingdom

[3]Institute for Molecular Bioscience, Australian Research Council Centre of Excellence for Innovations in Peptide and Protein Science, The University of Queensland, Brisbane, Queensland 4072, Australia

* Correspondence should be addressed: Sónia T. Henriques

Email: sonia.henriques@qut.edu.au

ABSTRACT

Lactate dehydrogenase 5 (LDH5) is overexpressed in metastatic tumors and is an attractive target for anticancer therapy. Small molecule drugs have been developed to target the substrate/cofactor sites of LDH5, but none has reached the clinic to date, and alternative strategies remain almost unexplored. Combining rational and computer-based approaches, we identified peptidic sequences with high affinity towards a β-sheet region that is involved in protein-protein interactions (PPIs) required for the activity of LDH5. To improve stability and potency, these sequences were grafted into a cyclic cell-penetrating β-hairpin peptide scaffold. The lead grafted peptide, cGmC9, inhibited LDH5 activity *in vitro* in low micromolar range and more efficiently than the small molecule inhibitor GNE-140. cGmC9 inhibits LDH5 by targeting an interface unlikely to be inhibited by small molecule drugs. This lead will guide the development of new LDH5 inhibitors and challenges the landscape of drug discovery programs exclusively dedicated to small molecules.

INTRODUCTION

Cancer cells adapt their metabolism to sustain the high energy demand of continued proliferation. Instead of using oxidative phosphorylation as the main source of energy, cancer cells switch to glycolysis even when oxygen is available. This phenomenon, known as aerobic glycolysis, or the Warburg effect, is a metabolic hallmark of cancer.[1,2] By doing this, cancer cells produce energy at a faster rate than with oxidative phosphorylation, obtain intermediates for biosynthesis of macromolecules, and secrete glycolysis end-product lactate to the extracellular media.[3] Lactate generates an acidic microenvironment that facilitates tumor-associated inflammation, angiogenesis, and immunosuppression, all contributing to tumor survival.[4,5] In addition, reduced oxidative phosphorylation results in lower levels of reactive oxygen species (ROS) and better survival of cancer cells. Therefore, targeting the Warburg effect is an attractive strategy for cancer therapy.[6,7]

Human Lactate Dehydrogenase (LDH), and more specifically the isoform 5 (LDH5), plays an essential role in the Warburg effect by catalyzing the final step of glycolysis,[8] *i.e.* the conversion of pyruvate to lactate, coupled with the regeneration of NAD^+ from NADH (Figure 1A). There are two LDH subunits, noted A and B, which are encoded by distinct genes, noted *LDHA* and *LDHB*, respectively. The subunits can assemble into five active tetrameric isoforms- LDH1: 4B, LDH2: 3B/1A, LDH3: 2B/2A, LDH4: 1B/3A and LDH5: 4A.[9] The homotetramers LDH1 and LDH5 are metabolically more active than the other isoforms and catalyze the interconversion of pyruvate to lactate in opposite directions[10] (Figure 1B).

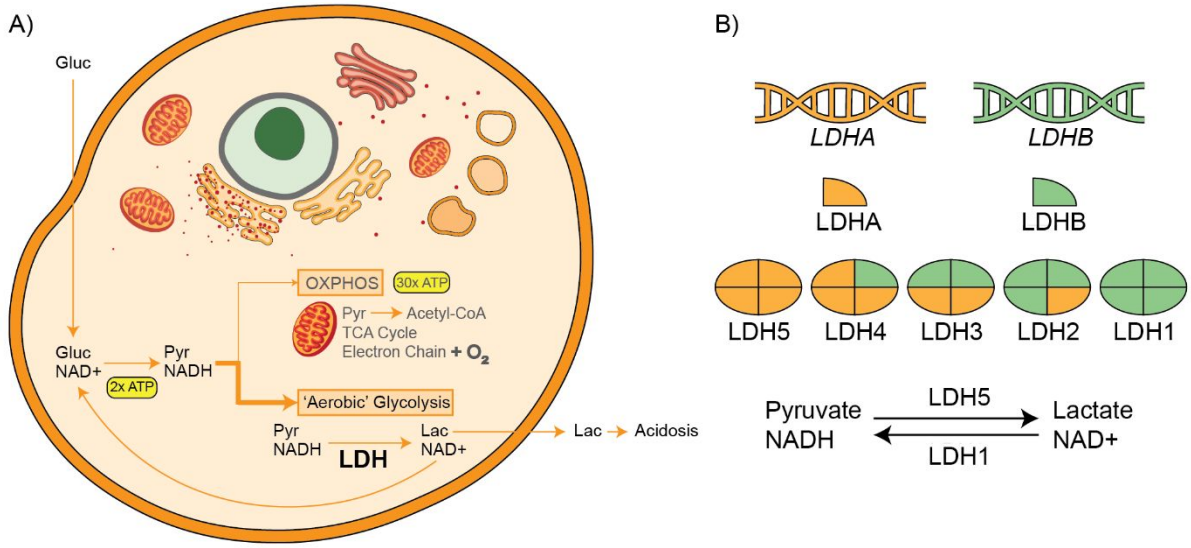

Figure 1: LDH5 as a target for anticancer therapy. (A) Cancer cells undergo metabolic changes relative to normal cells: glucose is mainly consumed via glycolysis even when oxygen is available, instead of the more efficient oxidative phosphorylation pathway. This phenomenon provides several advantages for cell proliferation including secretion of lactate to the extracellular media, which can lead to inflammation, angiogenesis and immunodepression. Lactate dehydrogenase (LDH) plays a key role by catalyzing the final step of glycolysis. (B) LDH is a tetramer and it includes five isoforms (LDH1–LDH5), formed by the five possible combinations of two subunits, *i.e.* LDHA and LDHB, which are encoded by the genes *LDHA* and *LDHB*, respectively. LDH5 is most active at catalyzing the conversion of pyruvate to lactate coupled with the oxidation of NADH into NAD^+, which is the final step of glycolysis. LDH1 is most active at catalyzing the opposite reaction.

LDH5 is overexpressed in many tumors, particularly in those that are highly aggressive and metastatic.[11] Thus, LDH5 has been identified as a biomarker for poor prognosis in a wide range of cancers, including pancreatic cancer, non-small-cell lung cancer, lymphoma, and brain metastases.[12-19] Of relevance, elevated LDH5 is also correlated with resistance against radiotherapy,[20] immunotherapy, and targeted chemotherapy, *e.g.* vatalanib that targets VEGF receptors and inhibits angiogenesis, or dabrafenib that inhibits B-RAF in melanoma patients

with mutated B-RAF V600E.[21] The pathways involved in the expression of LDH5 uphold the role of this enzyme in cancer. The *LDHA* gene is upregulated by the hypoxia inducible factor 1 (HIF1), which is constitutively elevated in cancer cells, and c-Myc, a well-known oncogenic transcription factor involved in cell division and proliferation.[19]

The role of LDH5 in cancer initiation, maintenance and progression was demonstrated by studies targeting the enzyme via chemical inhibition,[22,23] silencing technologies,[24-26] or genetic knock-out[27] both *in vitro* and *in vivo*. Impaired LDH5 activity reduces aerobic glycolysis and severely impacts cell proliferation. Some studies also showed an increase in oxidative phosphorylation, which leads to tumor regression via apoptosis induced by oxidative stress.[22-26] Together with the fact that congenital LDH5 deficiency in humans is not associated with a pathological phenotype,[28] there is abundant evidence to support LDH5 as a potential target for cancer therapy.[29]

Much effort has been expended by academia and pharmaceutical companies to develop LDH5 inhibitors. A large number of small molecules, either synthetic or isolated from natural sources, were reported to reduce LDH5 activity by competing with pyruvate and/or NADH for the active site.[30] Oxamate, a natural analog of pyruvate, was the first inhibitor described and it showed suppression of cell proliferation in breast cancer cells.[31] However, it is a weak inhibitor with low cell-penetration properties. FX11[22] and GNE-140[32,33] were discovered by high-throughput screening and achieved very high potencies in *in vitro* enzymatic assays. GNE-140 also showed micromolar inhibition of cell proliferation and good oral bioavailability in mice.[23,34] More recently, and because of the development of high-throughput screening technologies, new molecules have been reported to inhibit LDH5 in the nanomolar range, *e.g.* pyrazole-based inhibitors.[35,36] However, further research is needed to assess the viability of these molecules against *in vitro* biological systems and animal models. To date, no LDH5 inhibitor has progressed through clinical studies owing to low potency *in vivo* or toxicity caused

by cross-reactivity of NADH competitors. Alternative strategies to inhibit LDH5 remain almost unexplored.[37]

Because LDH5 is only active as a tetramer,[38,39] we propose targeting protein-protein interactions (PPIs) involved in the oligomerization of LDH5 thereby preventing its enzymatic activity. LDHA subunits assemble through large and highly dynamic interfaces, which are unlikely to be inhibited by small-molecule drugs. Peptides are emerging as an attractive alternative to small-molecule drugs to target PPIs, as they can achieve high specificity due to their larger interface of interaction,[40-43] can be chemically stabilized, for example via backbone cyclization, chemical staples, disulfide bonds, or the introduction of non-natural amino acids,[44,45] and can acquire the ability to cross cell membranes (*e.g.* via conjugation with cell penetrating peptides).[46] In addition, peptides also hold other advantages such as low toxicity, ease of synthesis, tumor penetrability, and lower potential to develop drug-resistance.[47] Hence, we hypothesize the use of peptides as alternative therapeutic leads to inhibit the enzymatic activity of LDH5.

In this study, we designed a series of β-hairpin peptides to inhibit the activity of LDH5 by preventing the oligomerization of its subunits, especially through disruption of a β-sheet located at the interface. Our work combines computer-based predictions with rational design and grafting into cyclic, stable peptide scaffolds. The designed peptides had low micromolar affinity for LDHA subunits and an ability to inhibit LDH5 enzyme activity in the low micromolar range. This approach validates the targeting of tetramerization as an alternative strategy to inhibit LDH5 activity.

RESULTS & DISCUSSION

Identifying the interface to target

The active tetrameric structure of LDH5[10] is formed by the dimerization of two LDHA subunits followed by dimerization of dimers (Figure 2A). Dimers are not catalytically active,[48] so we hypothesized that it would be possible to inhibit LDH5 activity by interfering with the dimer:dimer interface, which has lower affinity and greater surface exposure than the interface between subunits of the dimers. By examining the crystal structure of LDH5 (PDB ID: 1i10), we identified a region of interaction between dimers that includes residues 6 to 20 in the N-terminal arm and residues 297 to 305 from the adjacent subunit. The main contacts between these regions occur through an antiparallel β-sheet formed between two β-strands (residues 8 to 13 and 300 to 305), each contributed to by a different subunit (Figure 2B). LDHA and LDHB have high sequence and structural homology but not in the region involved in the dimer:dimer interface (Figure 2C).

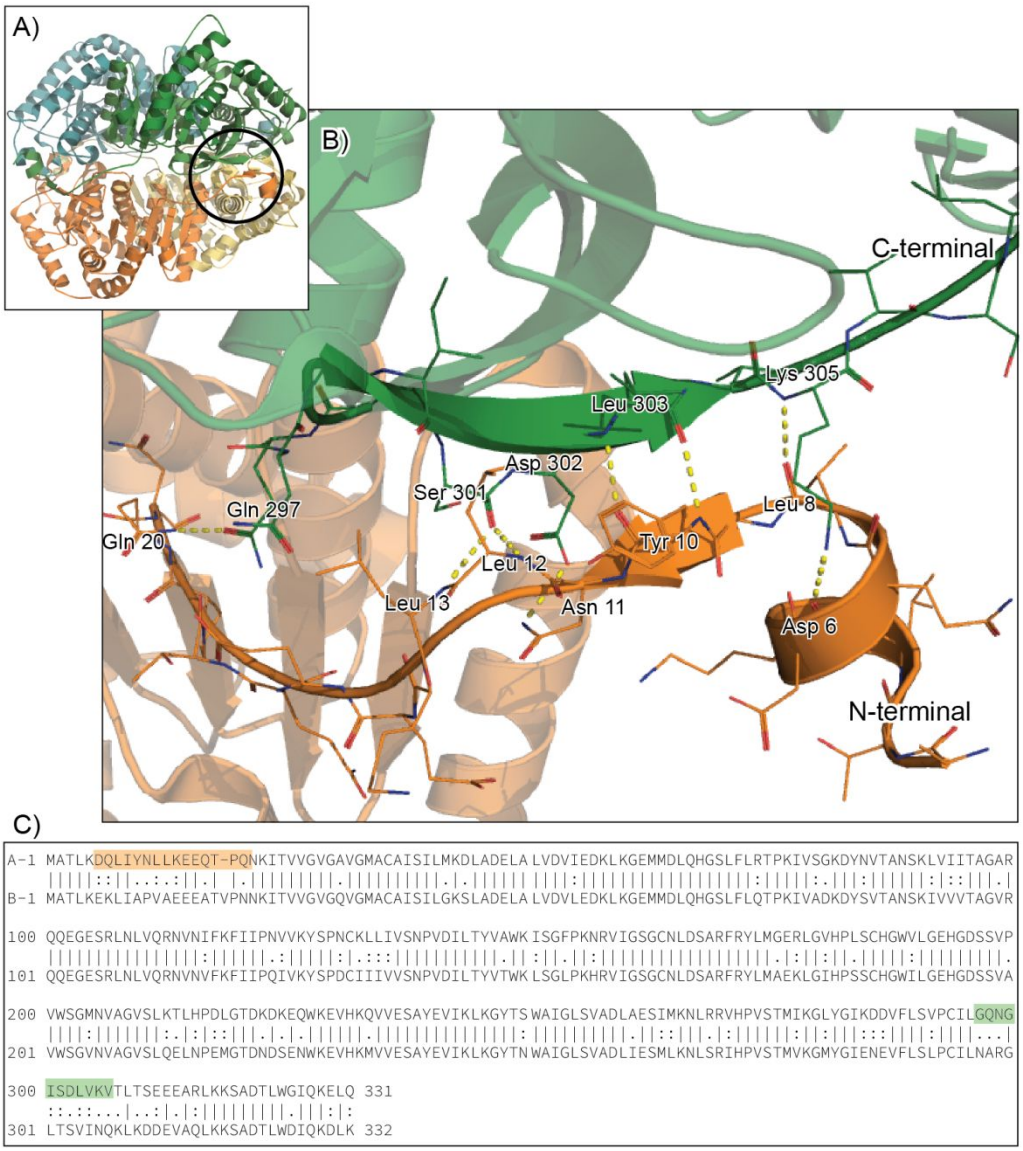

Figure 2: Characterization of the dimer:dimer interface of LDH5. (A) Tetrameric structure of LDH5 (PDB identifier 1i10); the tetramer is formed as a dimer of dimers[49], with the first two dimers to be formed shown in orange/yellow and green/blue. The region involved in the dimer:dimer interaction is circled in black. (B) Close-up view of the main dimer:dimer interface of LDH5, the N-terminal β-strand (orange; positions 7–12) of one LDHA interacts with the C-terminal β-strand of a different LDHA subunit (green; positions 300–305) by forming an inter-chain hydrogen-bond-stabilized β-sheet. (C) Sequence alignment between LDHA and LDHB. The residues that constitute the interface are shown in panel B with N-terminal and C-terminal β-strands highlighted in orange and green, respectively.

Targeting the dimer:dimer interface of LDH5 as a strategy to inhibit the formation of the active tetrameric LDH5 is supported by other studies. Depletions or substitutions at the N-terminal arm of LDHA compromise the stability of tetrameric LDH5 and, consequently, its enzymatic activity.[39,50] Furthermore, phosphorylation of Tyr10, which is also located in the N-terminal arm, increases the activity of LDH5 by enhancing tetramer formation. The single mutation Y10F increases mitochondrial activity in response to reduced glycolytic activity, and reduces proliferation and invasion of cancer cells.[51,52] Molecular dynamics simulations also suggested that the N-terminal arm is essential for the stabilization of tetrameric LDH5,[53] and peptides designed *in silico* to target this interface showed a reduction in the average size of LDH5 in solution suggesting loss of tetrameric form.[53] Overall, targeting the dimer:dimer interface is a promising strategy to inhibit enzymatic activity of LDH5.

Enzymatic assay to follow inhibition of tetramerization

To evaluate the ability of peptides to inhibit LDH5, we optimized a protocol previously employed to study the oligomeric structure of LDH5 and its relationship with enzymatic activity.[49,54,55] Under acidic conditions (pH 2.5), the protonation of amino acid side chains causes a decrease in hydrogen bonding, and LDH5 becomes partially denatured, which involves the loss of its quaternary structure and enzymatic activity, and also the partial loss of tertiary structure.[54] However, on bringing the solution back to physiological pH (pH 7.4) after a short incubation, LDHA subunits refold, reassociate into tetrameric LDH5, and consequently LDH5 recovers enzymatic activity (Figure 3A). Enzymatic activity was measured *in vitro* by adding substrates pyruvate and NADH, and monitoring the consumption of NADH by fluorescence emission intensity (λexcitation = 340 nm, λemission = 450 nm) over time. After 2 min at acidic pH followed by 120 min at physiological pH, LDH5 recovered more than 80% of its original enzymatic activity, as measured at the linear phase of the reaction (10 mins, 70% of substrate consumed) (Figure 3B). Peptides at varying concentrations were added at the start

of the reassociation step, and their ability to inhibit LDH5 tetramerization was measured by enzymatic activity and comparison with a positive control. Dose-response curves were fitted to determine the peptide concentration required to inhibit 50% of LDH enzymatic activity (IC_{50}). The assay was performed in the presence of 0.05% (w/v) bovine serum albumin (BSA) to exclude any non-specific inhibition on the re-folding or reassociation steps.

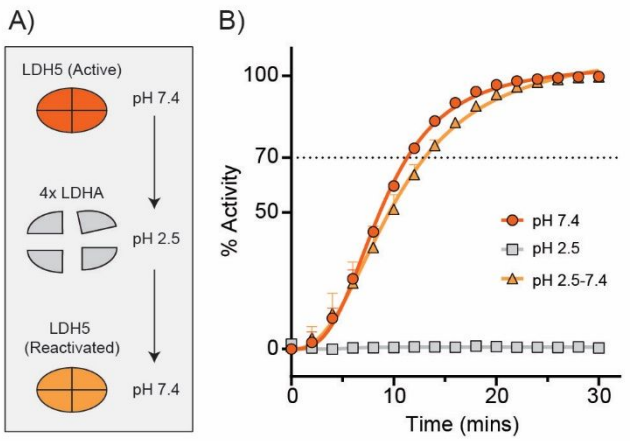

Figure 3: Enzymatic activity of LDH5 after pH-induced dissociation and reassociation. (A) The tetrameric structure of LDH5 is lost at acidic pH (pH 2.5) but bringing the sample back to physiological pH allows reassociation and reactivation of LDH5. (B) Enzymatic activity of LDH5 (10 nM) calculated from the consumption of NADH (300 μM) over time in an excess of pyruvate (3 mM). Decrease of NADH is measured by fluorescence intensity (λexcitation = 340 nm, λemission = 450 nm). The curve indicated as "pH 2.5-7.4" corresponds to LDHA that was reactivated at pH 7.4 after being dissociated into monomers at pH 2.5.

Design of inhibitory peptides

First generation: linear mimetics of both N-terminal and C-terminal regions

As a starting point, we synthesized a set of linear peptides that mimic N- or C-terminal regions involved in the dimer:dimer interface of LDH5. The amino acid sequences of these

peptides are shown in Figure 4A. They were synthesized using a rink amide resin, and their mass and purity were confirmed by analytical-HPLC and MS (Table S1, Figure S1). Peptides N1, N2 and N3, which mimic different lengths of the N-terminal region, did not inhibit reactivation of LDH5 because the active tetramer is formed even in the presence of these peptides. However, the C-terminal mimetic C2 showed weak inhibition of LDH5 activity (Figure 4A,B). Peptides C1 and C2 contain the key residues involved in the interactions between LDHA subunits but C2 is larger, making it more likely to acquire secondary structure, such as the β-strand present in the native protein. Low potency can be explained by smaller size compared to the competitor (*i.e.* LDHA subunits), and/or difficulty to form a stable β-strand conformation which is challenging especially for short peptides. The activity of C2, however, suggests that mimicking the C-terminal region of LDHA subunits (*i.e.* targeting the N-terminal region) is the preferred option.

A)

	Peptide	Sequence	Mass	Charge	IC50 (μM)	95% CI
1st	C1	Acetyl- QNGISDLVK -NH2	1014.1	0	>40	-
	C2	Acetyl-KKLSVPCILGQNGISDLVK -NH2	2053.5	+2	>40	-
	N1	MATLKDQLIYNLLKE -NH2	1792.1	+1	>40	-
	N2	Acetyl- DQLIYNLLKEEQTPQ-NH2	1873.0	-2	>40	-
	N3	MATLKDQLIYNLLKEEQTPQ-NH2	2375.8	0	>40	-
2nd	C3	Acetyl- GNYTWL -NH2	793.9	0	>40	-
	N4	Acetyl- PVQRTG -NH2	697.8	+1	>40	-
		β-strand1 Loop1 β-strand2 Loop2				
3rd	cGm	G C RRL C YKQR C VTY C RGR	2199.7	+6	36.6	±4.6
	Gm	Z C RRL C YKQR C VTY C RGR	2170.4	+7	>40	-
	cTI	KWC FRV C YRGI C YRR C RG	2303.8	+6	29.1	±5.0
	TI	KWC FRV C YRGI C YRR C R	2264.8	+6	40.5	±10.9
	cGmC4	C RRL C YKQR C DLV C RGR	2106.6	+5	27.3	±4.2
	cGmC5	C RRL C YKQR C FTV C RGR	2126.6	+6	24.0	±4.3
	cGmN5	C RRL C YKQL C NYI C RGR	2126.6	+5	>40	-
	cGmN6	C RRL C YKQG C RQV C RGR	2063.5	+6	41.4	±2.7
4th	cGmC6	C RRL C DRFW C FTV C RGR	2155.6	+4	10.4	±1.8
	cGmC7	C RRL C TGQR C FTV C RGR	1993.4	+5	>40	-
5th	cGmC8	C RRL C YRGI C VTY C RGR	2056.5	+5	24.8	±3.4
	cGmC9	C RRL C YRFW C FTV C RGR	2203.7	+5	2.5	±0.3
	cGmC10	C RRL C DRFA C FTV C RGR	2040.5	+4	>40	-
	cGmC11	G C RRL C WFRY C FTV C RGR	2260.7	+5	4.5	±0.7
	GNE-140				4.9	±1.0

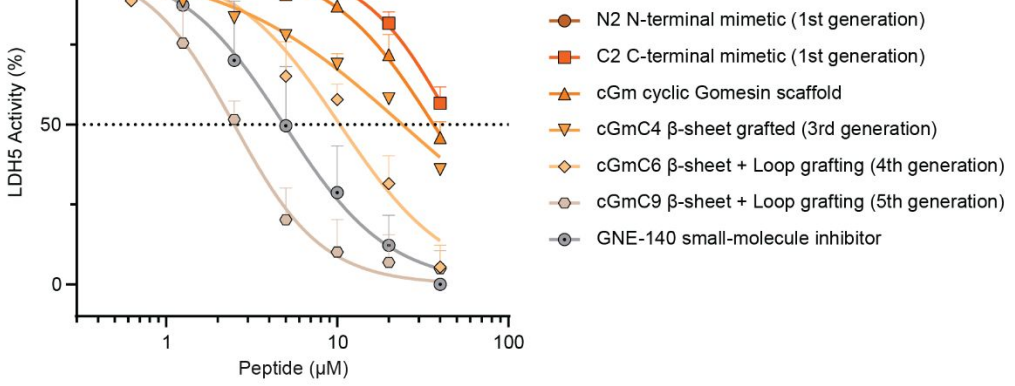

B)

Figure 4: Inhibition of LDH5 activity by designed peptides. (A) The table includes the generation of the design, peptide name, peptide sequence, mass, charge, peptide concentration (in μM) required to inhibit 50% of LDH5 enzymatic activity (IC50), 95% confidence interval, and schematic representation of the regions of interaction (orange) between the peptide inhibitor (green) and LDH5 (grey). First generation of peptides include linear mimetics of both N-terminal and C-terminal regions; second generation of peptides include computer-simulations using *Rosetta*; third generation of peptides include grafting into an antiparallel β-hairpin peptide scaffold (Z, on Gm, is N-terminal pyroglutamic acid);

fourth generation of peptides include computer-simulations using *Rosetta* on Loop 1 of the peptide scaffold; fifth generation of peptides include rational optimization. (B) Inhibition curves of selected peptides.

Second generation: design by computer-simulations using *Rosetta*

To address the lack of potency, we designed another series of peptides using *Rosetta* to predict sequences with optimal interaction against the regions of interest. *Rosetta* is a macromolecular modelling suite with an ability to design proteins with increased stability or affinity.[56,57] Using the crystal structure of LDH5[10] (PBD identifier 1i10), we used *Rosetta* to optimize the sequence of one of the β-strands (*i.e.* 8–13) for interaction with the other β-strand (*i.e.* 300–305), as well as other parts of the subunit located less than 10 Å from the β-sheet. The *FastRelax* protocol was employed during the design, enabling limited flexibility of the backbone conformation to adapt to change in side chain sequences. One hundred solutions were calculated for each β-strand, and we selected the most common occurring sequences. The identified sequences are PVQRTG for β-strand 8–13, and GNYTWL for β-strand 300–305, which were named N4 and C3, respectively (Figure S2).

N4 and C3 were synthesized and purified following the same protocols as in the previous generation of peptides (Table S1, Figure S1). Unfortunately, these linear peptides did not show inhibition of LDH5 reactivation (Figure 4A); we hypothesized that given their small size, these peptides are unlikely to acquire a stable β-strand conformation and are therefore inactive. We then aimed at developing larger stable peptides displaying stable β-strand conformations.

Third generation: using antiparallel β-sheet peptides as a scaffold

To investigate the importance of having a β-strand conformation to efficiently target the interface of interest, we grafted the above-mentioned small linear peptides into a peptide scaffold to induce the formation of a secondary structure. We selected gomesin (Gm), an antimicrobial peptide found in the haemocytes of the Brazilian spider *Acanthoscurria gomesiana*, as a scaffold.[58] This peptide possesses a β-hairpin structure, two-disulfide bonds, is amendable to modification, and can be chemically synthesized.[59] Furthermore, it has been successfully backbone cyclized to further increase its stability (cGm).[60] Another important characteristic of cGm as a scaffold is its capacity to penetrate cell membranes, which is at least partially dependent on the high number of positively charged residues present on its sequence.[61]

We chose residues 10–15 of cGm, which adopts a β-strand conformation, to engraft the LDHA-inhibitor sequences (Figure 4A). These cGm residues do not contain positively charged residues, and therefore we assumed that they are not as important for the cell penetrating properties of the scaffold.[61] In addition, we avoided modifying residues that are key for the structure, such as Cys 11, which is involved in a disulfide bond and, consequently, important for the stability of the molecule.[60] The designed peptides cGmC5 and cGmN6 (Figure 4A) were created by grafting the second generation of peptides predicted with *Rosetta* into cGm. To assess the quality of the computer predictions, we also designed cGmC4 and cGmN5 in which the native sequences of LDH5 were grafted into cGm (Figure 4A). These peptides were synthesized using 2-chlorotrityl chloride (2CTC) resin, backbone cyclized and oxidized as described by Cheneval et al.[62] Mass and purity were checked by analytical-HPLC and MS and the correct fold and secondary structure was confirmed by one-dimensional NMR spectroscopy (Table S1, Figures S1 & S3).

This series of peptides inhibited the enzymatic activity of LDH5 when added during the reassociation step. cGmC5, in particular, inhibited reactivation of LDH5 with an IC_{50} of 24.0 ± 4.3 μM (Figure 4A). These peptides were more potent than the first generation of linear

peptides (Figure 4B), suggesting the importance of a β-strand structure to target the dimer:dimer interface. However, cGmC5 and cGmN6 with computer-predicted sequences did not show a significant increase in inhibitory activity compared to the analogs cGmC4 and cGmN5, which display the native LDH5 sequences (Figure 4A). Furthermore, cGm and cyclic tachyplesin I (cTI),[63,64] a peptide with a β-hairpin structure similar to that of cGm, were used as a control, and also showed inhibition of LDH5 enzymatic activity. This suggests that the interaction between cGm, or cTI, with LDHA subunits lacks specificity and is most likely to occur through backbone contacts rather than side chain contacts. Non-backbone cyclized versions of gomesin and tachyplesin showed lower inhibitory activity than their cyclic analogs, probably due to the lower rigidity and stability of their β-hairpin structures[60,64] (Figure 4A).

Fourth generation: expanding the interface of interaction

To improve the inhibitory activity, we modelled the interaction between grafted cyclic peptides and LDH5 using *MODELLER*.[65] The models display several hydrogen bonds between the backbone of the cyclic peptides and LDH5. Interestingly, the loop formed with residues 7–10 of cGm is located near a flexible coil of LDH5 (residues 13–18) in the molecular models of the peptides targeting the N-terminal β-strand of LDH5 (*i.e.* cGmC4 and cGmC5). This proximity provided an opportunity to improve the potency by creating new interactions with LDH5. We used the *Fastrelax* protocol in *Rosetta* to optimize the interaction and predict the best combination of amino acids on these four positions of cGmC5. Within the 100 solutions that were calculated, the most frequent sequence predicted was DRFW (Figure S2). This sequence could affect the cell-penetrating properties of the designed peptides; the Asp residue would decrease the overall positive charge, which is detrimental to cell-penetration, but the Phe and Trp residues would increase the hydrophobicity, which typically favors membrane interactions and cell penetration. We made additional *in silico* predictions with *Rosetta* using the *Fixedbackbone* protocol, and the most common sequence across 100 calculations was

DGQR (Figure S2). However, we substituted the Asp residue, which is the most distant to LDH5, by a Thr residue aiming to maintain a higher overall positive charge of the peptide. The two corresponding analogs of cGmC5, which were named cGmC6 (DRFW sequence from *Fastrelax*) and cGmC7 (TGQR sequence from *Fixedbackbone*) respectively, were synthesized (Table S1, Figures S1 & S3), and their ability to inhibit reactivation of LDH5 measured. cGmC6 had an IC_{50} of 10.4 ± 1.8 μM, which is a remarkable improvement in potency compared to previous designs (Figure 4A,B).

Fifth generation: rational optimization of peptide leads

The next generation of analogs was designed using a rational approach applied to cGmC6. The increased inhibitory activity of cGmC6, compared to cGmC5, indicated that residues in loop 1 might interact with LDHA subunits and therefore could be modified to further improve inhibitory activity. Since cTI and TI inhibit the enzymatic activity of LDH5 (Figure 4A), we incorporated residues from these peptides into cGmC6. TI is not backbone cyclic and has only one loop (*i.e*. loop 1: YRGI), whereas cTI has two loops of four residues each (*i.e.* YRGI in loop 1 and RGKW in loop 2). We hypothesized that loop 1 is involved in the interaction with LDHA subunits because cTI and TI inhibit the activity of LDH5 with similar efficacy. Accordingly, we designed and synthesized two analogs of cGmC6: cGmC8 (Table S1, Figures S1 & S3), in which the interacting loop was replaced with the loop of cTI (YRGI); and cGmC9 (Table S1, Figures S1, S3 & S4), a hybrid sequence in which the interacting loop (YRFW) displays a mixture of residues from cTI and from cGmC6 (Figure 4A).

cGmC9 is more potent at inhibiting the reactivation LDH5 enzymatic activity (IC_{50} = 2.5 ± 0.3 μM), than the "gold standard" small molecule inhibitor GNE-140 (IC_{50} = 4.9 ± 1.0 μM; Figure 4A,B). To further explore the inhibitory activity of cGmC9 and better understand

structure-activity relationships, we synthesized the analog cGmC10, in which the Trp residue located in loop 1 of cGmC6 and cGmC9 was replaced with an Ala, and the analog cGmC11 to include scrambled residues in the loop region, WFRY instead of YRFW (Table S1, Figures S1 & S3). cGmC10 showed a dramatic decrease in inhibitory activity compared to cGmC9 (Figure 4A) even though NMR data suggested that cGmC10 maintains the β-hairpin structure of its analog peptides (Figure S3). This finding suggests that Trp10 is important for the interaction with LDH5. Despite showing a 2-fold drop in potency (IC_{50} = 4.5 ± 0.7 μM), cGmC11, the peptide with the active loop scrambled, was still very potent (Figure 4A). Computer-predicted interactions by *MODELLER*[65] showed a hydrogen bond between residue 10 in loop 1 of both cGmC9 and cGmC11 and Leu12 of LDH5, which was not formed between cGmC10 and LDH5 (Figure S5). Tyr10 in cGm11 could form the same hydrogen bond as that of Trp10 in cGm9, and the formation of this hydrogen bond potentially contributes to give similar potency to the two peptides, supporting the importance of having a Trp and/or Tyr in loop 1.

Binding and mechanism of action of LDH5 inhibitors

Fluorescence polarization experiments were done to investigate the relative affinity of the cGm-based inhibitors for LDH5. We used [G1K, K8R]cGm, a cGm analog previously characterized in our group [60] that includes a Lys residue in loop 2 so it can be labeled by amide bond ligation with the fluorophore Alexa Fluor®488 ([G1K, K8R]cGm-A488).[61] Despite being less potent than cGmC9, [G1K, K8R]cGm also showed inhibition of LDH5 reactivation (Figure 5A), which indicates binding between the peptide and LDH5. Given its small size, [G1K, K8R]cGm-A488 (~2 kDa) rotates faster in the unbound state than when bound to a much larger protein, such as LDHA (37 kDa), which results in its fluorescence emission becoming more polarized when in the bound state compared to unbound.

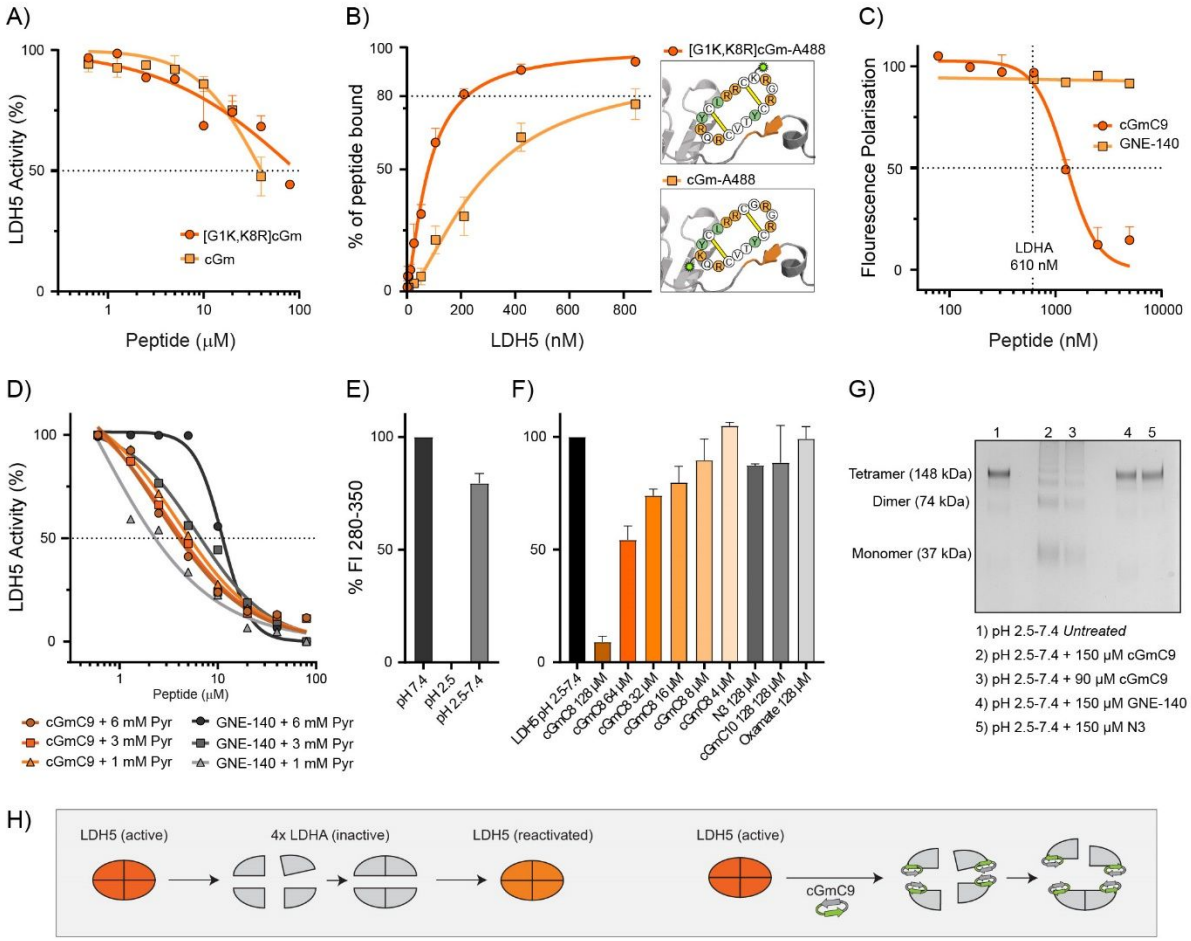

Figure 5: cGm-based inhibitors bind to LDH5 and affect the tetramerization of the enzyme. (A) Inhibition of LDH5 activity after pH-induced dissociation and reassociation by [G1K, K8R]cGm and cGm. (B) Binding curves between LDH5 and peptides cGm or [G1K, K8R]cGm labeled with Alexa Fluor®488. The binding was measured as an increase in fluorescence polarization (λ(excitation) = 485 nm, λ(emission) = 520 nm) and B_{max} of the curve is established as 100% of peptide bound to protein. The legend includes an illustration of the peptide sequences, the localization of the fluorophore, and a schematic representation of the proposed binding mode. (C) Competition assay between [G1K, K8R]cGm-A488 and specific LDH5 inhibitors. 100% of fluorescence polarization was established as intensity obtained by 152.5 nM LDH5 and 12 nM of [G1K, K8R]cGm-A488. (D) Inhibition of LDH5 activity after pH-induced dissociation and reassociation by cGmC9 and GNE-140 under different concentrations of pyruvate. All samples were normalized against the enzymatic activity of an untreated control sample. (E) Tryptophan fluorescence emission intensity (FI; λexcitation = 280 nm, λemission = 350 nm) of LDH5 samples at different pH conditions. FI values obtained at pH 7.4 were established

as 100%. (F) Effect of inhibitors on tryptophan fluorescence of LDH5 (0.6 μM) after pH-induced dissociation and reassociation. (G) SDS-PAGE of pH-induced dissociated and reassociated LDH5 (1.3 μM) treated with inhibitors. After treatment, samples were cross-linked with glutaraldehyde to covalently bind any interactions between LDHA subunits that would be lost due to denaturing conditions of the gel. (H) Schematic illustration of the dissociation and re-association of LDH5 and the effect of inhibitor cGmC9, which targets oligomerization of the active enzyme.

We established a binding curve between [G1K, K8R]cGm-A488 and LDHA subunits by measuring fluorescence polarization after pH-induced dissociation and reassociation of LDH5. The binding curve reaches a plateau phase when most of the peptide molecules are bound to LDHA subunits. The fluorescence polarization signal at binding saturation was calculated by a non-linear regression and set as 100% of peptide-protein binding. A LDH5 concentration of 80 nM was enough to obtain 50% binding of 12 nM [G1K, K8R]cGm-A488 (Figure 5B). Native cGm, also labeled with Alexa Fluor®-488 (cGm-A488), did not reach the plateau phase of the curve under the same conditions. This indicates lower binding affinity to LDH5 than [G1K, K8R]cGm-A488 and it might result from the position of the Lys residue and the conjugated fluorophore located in loop 1 of cGm, which may interfere with the interaction between the peptide and LDHA subunits.

To further study the mechanism of action of cGm-based LDH5 inhibitors, we performed competition experiments with [G1K, K8R]cGm. If the loss of activity observed in enzymatic assays is related to impaired tetramerization, a non-labeled inhibitor would compete for the same binding site releasing [G1K, K8R]cGm-A488 and, as a consequence, reducing fluorescence polarization. We extrapolated the required conditions to achieve 80% of peptide binding (*i.e.* 12 nM [G1K, K8R]cGm-A488 and 152.5 nM LDH5) and co-incubated with peptide inhibitors at varying concentrations. Co-incubation with cGmC9 dramatically reduced

fluorescent polarization in a concentration dependent manner. 1.28 μM of cGmC9 was needed to reduce fluorescence polarization to half, but this value is not indicative of the potency of the inhibitor because there is an excess of LDH5 in solution. In fact, fluorescence polarization levels decrease abruptly when cGmC9 reaches the same concentration of LDHA subunits in solution (610 nM), suggesting a 1:1 interaction. Interestingly, GNE-140 which displayed potent inhibitory activity in enzymatic assays, did not affect the levels of fluorescence polarization even when incubated at higher concentrations than LDH5. This confirms that cGm-based inhibitors and GNE-140 have different binding sites and supports distinct mechanisms of action (Figure 5C).

Enzymatic assays using different concentrations of pyruvate provide further support that cGmC9 and GNE-140 have distinct mechanisms of action (Figure 5D). The inhibitory activity of GNE-140 decreases with increasing concentration of LDH5 or of pyruvate, suggesting a mechanism whereby the inhibitor competes with the substrate to bind to the active site. By contrast, the inhibitory activity of cGmC9 is independent of pyruvate concentration (Figure 5D), and only competes against other LDHA subunits.

To further demonstrate that cGm-based LDH5 inhibitors bind and destabilize LDH5, we measured intrinsic Trp fluorescence of LDH5, which can be used to determine the conformational state of a protein. When a protein is folded, Trp residues typically localize in the hydrophobic core of the protein, instead of being exposed to the surrounding aqueous medium. In the particular case of LDH5, each LDHA subunit contains six Trp residues, three of them located in the core of the protein and three at the dimer:dimer interface. Therefore, when LDH5 is not in a tetrameric form, Trp residues located at the dimer:dimer interface become exposed to a more aqueous environment. Trp fluorescence emission is dependent on the environment, with the quantum yield reduced when moving from hydrophobic towards polar environments. Thus, when Trp residues at the dimer:dimer interface become exposed to

polar solvents, the fluorescence emission decreases, as confirmed when comparing LDH5 at pH 7.4 and pH 2.5 (Figure 5E).

We used peptide cGmC8 for this experiment, despite it not being the most potent inhibitor, because it does not contain Trp residues that cause background signal and mask the actual measurement of LDH5 intrinsic fluorescence. The same pH-based approach described for the enzymatic assays was used to reproduce the process of tetramerization. In accordance with the enzymatic activity, reassociated LDH5 recovered 90% of its original fluorescence compared to dissociated LDH5 at acidic pH (Figure 5E). cGmC8 prevented the recovery of fluorescence in a concentration-dependent manner, 64 μM being the required concentration to inhibit 50% of LDH5 reassociation (Figure 5F). N3 and cGmC10, which did not show inhibition of the enzymatic activity (Figure 4A), were used as controls and they did not affect the reassociation of LDH5. GNE-140 was not included as a control because it absorbs light at 280 nm, due to its aromatic rings, and interferers with the fluorescence emission of Trp residues. Instead, we used oxamate as the small molecule inhibitor control. Despite using high concentrations of oxamate, the recovery of fluorescence was not affected under the presence of the small molecule inhibitor.

The oligomerization state of LDH5 after treatment with the inhibitors (after pH-based dissociation/reassociation) was also investigated using SDS-PAGE separation (Figure 5G). We used glutaraldehyde as a cross-linker to covalently bind LDHA subunits that are successfully reassociated, because denaturing conditions of the gel would break the quaternary structure of the protein. The positive control (Lane 1) shows a high-mass band of 148 kDa, which corresponds to tetrameric LDH5. Existence of an active tetrameric structure agrees with the enzymatic assay, in which LDH5 is inactivated at pH 2.5 but recovers most of its activity at pH 7.4 (Figure 3). When LDH5 is treated with cGmC9 during the reassociation step, the band distribution is altered; the tetrameric band is very subtle whereas bands at molecular weights

close to that of the dimeric (74 kDa) and monomeric (37 kDa) forms become the most intense ones. The N-terminal arm of LDH5 is involved in the overall stability of the enzyme,[39] and deletions of this region result in the formation of dimeric and monomeric subunits, as reported in previous studies.[50] cGmC9 binds to the N-terminal arm of LDHA in its monomeric form and therefore this interaction is likely to affect the whole reassociation process, including the monomer:monomer dimerization (Figure 5H), which explains the existence of a band at the molecular weight of a monomeric form. The second dimerization (*i.e.* dimerization of dimers) is likely to be directly affected by cGmC9 as it binds to a key interface of this interaction, explaining the band at the molecular weight of the dimeric form and disappearance of the tetrameric form (see Figure 5G,H).

Treatment with the small-molecule inhibitor GNE-140 (Lane 4), which showed potent inhibition of LDH5 activity through NADH competition, did not affect the band distribution compared to untreated LDH5 and showed a very intense band at 148 kDa, suggesting a dominant presence of tetrameric LDH5. Peptide N3 (Lane 5), which did not show inhibitory activity (Figure 4A), also showed similar band distribution. These results confirm the ability of cGmC9 to prevent oligomerization of LDH5 as the mechanism of action to inhibit its enzymatic activity (Figure 5H).

CONCLUSIONS

We have discovered a series of peptides that successfully inhibit the activity of LDH5. The inhibitors presented in this study were optimized by starting with linear mimetic sequences, followed by grafting into stable peptide scaffolds, rational design, and by computer-based strategies. Peptide cGmC9 showed exceptional potency with a lower IC_{50} than GNE-140, a ‘gold standard’ small molecule inhibitor of LDH5. The mechanism of action of these

peptides to achieve inhibition of LDH5 is based on modulation of PPIs. Interestingly, the interface of interest is a β-sheet, which is targeted by β-hairpin peptides, an uncommon strategy due to the challenges of achieving high specificity and potency.

Previous studies reported peptide inhibitors of LDH5 able to affect the average particle size in solution, suggesting they affect the tetrameric structure of the enzyme.[53] A recent study of the tetramerization of LDH1, showed that designed stapled α-helical peptides are able to bind and destabilize LDH1. Interestingly, one of the peptides also affected the reassociation of rabbit LDH5 at a concentration of 300 μM as measured by tryptophan fluorescence.[66] However, to our knowledge, this is the first time a peptide inhibitor has been designed to target human LDH5 tetramerization and shown to inhibit its enzymatic activity. cGm-based inhibitors showed a different binding site and mechanism of action than small molecule inhibitors. The exact binding location of the peptides was not confirmed in this study and would require a high-resolution structure of the peptide inhibitors with LDH5. However, the tetrameric structure of LDH5 was disrupted by the designed peptides, as shown by tryptophan fluorescence experiments and by SDS-PAGE protein gels, which explains their inhibitory activity. Furthermore, molecular dynamic simulations showed binding of cGmC9 in the N-terminal region of LDHA and high stability of the cGmC9/LDHA complex, even when LDHA is phosphorylated at Tyr10 (Figure S6), a relevant post-transcriptional modification in the interface of interest that enhances tetramerization[51].

Overall, this study demonstrates that inhibiting PPIs involved in the tetramerization of LDH5 is a valid approach to inhibit the enzymatic activity of LDH5. Furthermore, the optimization of peptide inhibitors over several generations revealed important information about the dimer:dimer interface of LDH5, for instance, the relevance of a stable β-strand on the peptide inhibitors to be able to 'compete' with PPIs at the interface of LDHA subunits. We also found that targeting the N-terminal region of the dimer:dimer interface, instead of the C-

terminal region, is more successful. This is probably due to an extended coil at the N-terminal arm, which provides a larger area of interaction and can increase the specificity of the inhibitors. Specificity and potency of the best inhibitor can be further improved using high-throughput screening strategies (*e.g.* peptide libraries).

cGmC9 and other peptides designed in this study utilized a cGm scaffold. Despite introducing a range of modifications to cGm, cGmC9 still displays two disulfide bonds and maintains the β-hairpin structure of its precursor scaffold (Figure S4 & S7). Five of the six positively charged residues of cGm, which are important for its cell-penetrating properties,[61] were kept in cGmC9 (Figure S7). The stability and cell-penetrating properties of cGm set an exciting background for future optimization of these peptide inhibitors as therapeutics against LDH5, which is found in the cytosol.

EXPERIMENTAL SECTION

Peptide synthesis, folding, purification, and labelling. Linear peptides (*i.e.* C1, C2, C3, N1, N2, N3, N4, Gm, and TI) were synthesized using Fmoc solid-phase chemistry and a rink amide resin. Protective groups were cleaved in trifluoracetic acid (TFA) containing 2.5% (v/v) triisopropylsilane and 2.5% (v/v) H_2O. Cyclic peptides (*i.e.* cGm, cTI, cGmC4, cGmC5, cGmN5, cGmN6, cGmC6, cGmC7, cGmC8, cGmC9, cGmc10, cGmC11 and cGmC9K) were synthesized using Fmoc solid-phase chemistry and a 2-chlorotrityl chloride (2CTC) resin, cyclized, and folded according to the methodologies described by Cheneval et al.[62] All peptides were purified using RP-HPLC. Correct mass and purity of ≥95% was confirmed by LC-MS for all peptides (Table S1, Figure S1). Correct folding of peptides was confirmed using ^{1}H NMR spectroscopy on a Bruker Avance 600 MHz spectrometer by comparing the spectra to that of cGm (Figure S2).[60] Concentration of peptides in solution was determined by reading

absorbance at 280 nm with a nanodrop except for peptides C1, C2, N4, cGmC7, and cGmC10 which were determined by direct weighing due to their lack of aromatic residues. Some peptides were labelled with Alexa Fluor® 488 (A488) on the side chain of a single Lys residue through amide-bond ligation. Dried peptides (~0.5 mg) were solubilized in 78 µL *N,N*-dimethylformamide (DMF) and incubated with 20 µL of 12 mM Alexa Fluor®488 sulfodichlorophenol ester (Life Technologies, #A30052) and 2 µL of *N,N*-diisopropylethylamine (DIPEA). After 2 hours, labelled peptides were purified, and mass/purity were confirmed. Concentration of labelled peptides in solution was determined by reading absorbance at 495 nm with a nanodrop (ε_{495} = 71,000 M^{-1} cm^{-1}).

Enzymatic assays. Recombinant human LDHA and LDHB were purchased from Abcam (#ab93699 and #ab96765, respectively). The active protein was diluted to 900 nM in 0.01 M phosphate buffer (pH 7.4) 1 mM EDTA 0.05% BSA. 5 µL of protein solution was transferred into a Nunc™ 96-well polypropylene microplate (#249944) and incubated with 10 µL of 0.1 M glycine buffer (pH 2.5) 0.05% BSA (w/v) for 2 minutes. Afterwards, 20 µL of 0.25 M phosphate buffer (pH 7.6) 1 mM EDTA 0.05% BSA containing different concentrations of peptide was added to the samples. After incubation for 2 hours at room temperature, 10 µL of sample was transferred into a Corning® black polystyrene 96-well microplate (#CLS3925) containing 90 µL of 0.25 M phosphate buffer (pH 7.6) 1 mM EDTA 0.05% BSA (w/v) per well. The enzymatic reaction was initiated by addition of 20 µL of substrate buffer containing 18 mM pyruvate and 1.8 mM NADH for a final concentration of 3 mM pyruvate and 0.3 mM NADH. The consumption of NADH was followed over time by measuring fluorescence emission intensity (λexcitation = 340 nm, λemission = 450 nm) with a PHERAstar microplate reader. To calculate the inhibitory activity of peptides, fluorescence emission intensity of the samples was compared directly to a positive control without inhibitors before reaching the plateau phase of the reaction (70% of substrate consumed).

Computer-based predictions. For the second generation of peptides, residues 8–13 and 300–305 of LDHA were selected as target regions for developing inhibitors. Residues located within 10 Å of the next chain, as shown in a crystal structure of LDH5 (PBD ID: 1i10), were also included in the predictions.[10] The *FastRelax* protocol of *Rosetta*, which optimizes backbone conformation during the design process, was used to predict sequences that target the regions of interest starting from native sequence of LDH5.[57,67] One hundred solutions were calculated, and the top occurring sequence was selected to be synthesized. For the fourth generation of peptides, which includes cGm-based peptides, molecular models of the interaction between cGmC5 and the target region of LDHA were computed using *MODELLER 9v20*[65] and two templates: the crystal structure LDH5 in its tetrameric form (PBD ID: 1i10) and the NMR solution structure Gm (PDB ID: 1kfp). These molecular models were then used to further optimize cGmC5 for interaction against LDHA using the *FastRelax* or the *Fixedbackbone* protocols implemented in *Rosetta*.[67,68] All parameters of these two protocols were kept to their default values. *Rosetta* version 2017.08.59291 was employed for these computations.

Fluorescence polarization. 10 µL of recombinant human LDH5 (#ab93699) was serially diluted two-fold in a Corning® half-area black polystyrene 96-well microplate (#CLS3694) in 0.01 M phosphate buffer (pH 7.4) 1 mM EDTA starting at 3.375 µM and incubated with 10 µL of 0.1 M glycine buffer (pH 2.5) for 2 minutes. Afterwards, 20 µL of 0.25 M phosphate buffer (pH 7.6) 1 mM EDTA containing 24 nM of labeled peptide with Alexa-Fluor®488 was added to the sample. The samples were incubated for 2 hours at room temperature. FP was measured (λexcitation = 485 nm, λemission = 520 nm) using a PHERAstar microplate reader. The FP values resulting in a curve were analyzed as a nonlinear regression - specific binding with Hill slope, and FP at saturation (FP_{max}, *i.e.* 100% of peptide bound) was calculated. FP values were then normalized to FP_{max} it being 100% of peptide bound to LDH5. 12 nM [G1K, K8R]cGm-A488 and 620 nM LDHA, which corresponds to 80% of peptide bound to LDHA, were the

conditions established to perform competition assays. To do that, the same protocol was followed but different concentrations of inhibitors were added at the start of the reassociation step, together with the 20 µL of 0.25 M phosphate buffer (pH 7.6) 1 mM EDTA containing 24 nM of labeled peptide with Alexa-Fluor®488.

Tryptophan fluorescence of LDH5. 10 µL of 4 µM recombinant human LDHA (#ab93699) was incubated with 20 µL of 0.1 M glycine buffer (pH 2.5) in a Corning® black polystyrene 96-well microplate (#CLS3925) for 2 minutes. Afterwards, 40 µL of 0.25 M phosphate buffer (pH 7.6) 1 mM EDTA containing different concentrations of peptide was added to the samples. After incubation for 2 hours at room temperature, fluorescence intensity was measured (λexcitation = 280 nm, λemission = 350 nm) using a PHERAstar microplate reader. Fluorescence intensity of controls without LDHA was measured and subtracted from the samples. The zero was set as fluorescence intensity measured at pH = 2.5. To measure the effect of peptides in the recovery of tryptophan fluorescence for the controls, the fluorescence intensity obtained with the control pH = 2.5 → 7.4 was used to define the maximum.

SDS-PAGE separation. 4 µL of recombinant human LDHA (#ab93699) was incubated with 4 µL of 0.1 M glycine buffer (pH 2.5) in a Corning® black polystyrene 96-well microplate (#CLS3925) for 2 minutes. Afterwards, 12 µL of 0.25 M phosphate buffer (pH 7.6) 1 mM EDTA containing different concentrations of peptide was added to the samples. After incubation for 2 hours at room temperature, 4 µL of 5% glutaraldehyde was added to the sample to act as a cross-linker. Samples were resuspended in NuPAGE LDS Sample Buffer and incubated at 85 °C for three minutes prior to SDS-PAGE analysis, performed in NuPAGE 4-12% Novex Bis-Tris gels and MES SDS running buffer (Invitrogen), following standard SDS-PAGE protocols.

Molecular dynamic simulations. The simulation was carried out in a water box using the Amber FF14SB forcefield and the Amber 20 molecular dynamics simulation package. Pressure and temperature were maintained to 1 atm and 300K using the Montercarlo barostat and Langevin thermostat, respectively. During the simulation, the Cα atoms of LDHA were restrained to their initial position but all other atoms were unrestrained.

Internalization assays. Internalization of cGm-A488 and of cGmC9K-A488, a cGmC9 analogue with a G1K mutation to enable fluorescently labelling through amide-bond ligation, was monitored using a BD LSRFortessa™ X-20 flow cytometer. MDAMB231 cells (*i.e.* triple-negative breast cancer) were seeded in 24-well plates (10^5 cells/well) and incubated for 24 h. Afterwards, labelled peptides diluted in medium without serum were incubated with cells for 1 h at 37 °C. Highest peptide concentration tested was 2 μM and 4 μM for cGm-A488 and cGmC9K-A488, respectively, and required serial dilutions to reach ~0 % internalization were included in the measurements. Peptides were incubated with cells in the absence of serum to avoid increased peptide uptake due to serum stimulating endocytic pathways. Cells were washed, trypsinized, washed again, and resuspended with cold PBS. Percentage of fluorescent cells was quantified by screening 10^4 cells/sample as previously described [69,61]

Serum stability assay. Human serum from male AB plasma (Sigma–Aldrich #H4522) was centrifuged at 17 000 *g* for 10 min to remove the lipid component, and the supernatant was incubated for 15 mins at 37 °C. Stability in 25% (v/v) serum was tested at a final peptide concentration of 200 μM in a total volume of 150 μL. The incubation time points included 0 and 24 h at 37 °C. Two additional early time points were included for N3 because the linear peptide was fully degraded after 24h. Serum proteins were precipitated by addition of TFA to a final concentration of 10% (v/v) followed by 10 min incubation at 4 °C. The samples were centrifuged at 17 000 *g* for 10 min. 40 μL aliquots of supernatant were taken out in triplicate from the samples and run on RP-HPLC using a linear 1 % min^{-1} gradient of 0–50 % solvent B.

The stability at each time point was calculated as the peak height of the serum-treated peptide on RP-HPLC at 215 nm as a percentage of the peak height of zero hours serum-treated peptides.

ASSOCIATED CONTENT

Supporting information

Supplementary Table and Figures. Table S1: Physicochemical properties of peptides; Figure S1: Analytical HPLC traces and mass spectra of all peptides; Figure S2: Peptide design solutions using *Rosetta;* Figure S3: ^{1}H NMR spectra of oxidized cGm-based active peptides; Figure S4: NMR α-H secondary chemical shifts of cGm and cGmC9; Figure S5: Molecular model of the interaction between cGm-based inhibitors and LDHA predicted using *MODELLER* 9v20 (PDF); Figure S6: Molecular dynamics simulation of cGmC9 in complex with LDHA; Figure S7: Cell-penetrating properties and serum stability of cGmC9 and its precursor cGm.

Molecular formula strings of all compounds.

Author contributions

FBN: Conceptualization, Methodology, Investigation, Visualization, Data Curation, Writing- Original Draft, Writing- Review & Editing. JMM: Investigation, Writing- Review & Editing. LYC: Methodology, Investigation, Writing- Review & Editing. DJC: Resources, Supervision, Funding acquisition, Writing- Review & Editing. QK: Conceptualization, Methodology, Investigation, Supervision, Writing- Review & Editing. STH: Conceptualization, Supervision, Methodology, Data Curation, Resources, Funding acquisition, Writing- Review & Editing.

ACKNOWLEDGEMENTS

This project was supported by an Australian Research Council (ARC) Future Fellow (FT150100398) awarded to STH. FNB was supported by a Queensland University of Technology Postgraduate Research Award Scholarship. JMM is supported by the Biotechnology and Biological Sciences Research Council (BB/T018275/1 and BB/R017956/1) and Cancer Research UK (A26941). The Translational Research Institute is supported by a grant from the Australian Government. DJC is an ARC Australian Laureate Fellow (FL150100146). This work was supported by access to the facilities of the Australian Research Council Centre of Excellence for Innovations in Peptide and Protein Science (CE200100012).

ABBREVIATIONS

2CTC, 2-chlorotrityl chloride; BSA, bovine serum albumin; cGm, cyclic gomesin; cTI, cyclic tachyplesin; DIPEA, *N,N*-diisopropylethylamine; DMF, *N,N*-dimethylformamide; EDTA, ethylenediaminetetraacetic acid; FI, fluorescence emission intensity; Gm, gomesin; HIF1, hypoxia inducible factor 1; HPLC, high performance liquid chromatography; LDH, lactate dehydrogenase; NAD, Nicotinamide adenine dinucleotide; NMR, nuclear magnetic resonance; PPI, protein-protein interaction; ROS, reactive oxygen species; SDS-PAGE, sodium dodecyl sulphate-polyacrylamide gel electrophoresis; TFA, trifluoroacetic acid; TI, tachyplesin; VEGF, vascular endothelial growth factor.

REFERENCES

1. Warburg, O. Respiratory impairment in cancer cells. *Science* **1956,** *124*, 269-270.

2. Warburg, O. Origin of cancer cells. *Science* **1956,** *123*, 309-314.

3. Lu, J. R. The Warburg metabolism fuels tumor metastasis. *Cancer Metast Rev* **2019,** *38*, 157-164.

4. Ippolito, L.; Morandi, A.; Giannoni, E.; Chiarugi, P. Lactate: A metabolic driver in the tumour landscape. *Trends Biochem Sci* **2019,** *44*, 153-166.

5. de la Cruz-Lopez, K. G.; Castro-Munoz, L. J.; Reyes-Hernandez, D. O.; Garcia-Carranca, A.; Manzo-Merino, J. Lactate in the regulation of tumor microenvironment and therapeutic approaches. *Front Oncol* **2019,** *9*, 1143.

6. Ganapathy-Kanniappan, S. Molecular intricacies of aerobic glycolysis in cancer: Current insights into the classic metabolic phenotype. *Crit Rev Biochem Mol Biol* **2018,** *53*, 667-682.

7. Zdralevic, M.; Vucetic, M.; Daher, B.; Marchiq, I.; Parks, S. K.; Pouyssegur, J. Disrupting the 'Warburg effect' re-routes cancer cells to OXPHOS offering a vulnerability point via 'ferroptosis'-induced cell death. *Adv Biol Regul* **2018,** *68*, 55-63.

8. Augoff, K.; Hryniewicz-Jankowska, A.; Tabola, R. Lactate dehydrogenase 5: An old friend and a new hope in the war on cancer. *Cancer Letters* **2015,** *358*, 1-7.

9. Markert, C. L. Lactate dehydrogenase isozymes: Dissociation and recombination of subunits. *Science* **1963,** *140*, 1329-1330.

10. Read, J. A.; Winter, V. J.; Eszes, C. M.; Sessions, R. B.; Brady, R. L. Structural basis for altered activity of M- and H-isozyme forms of human lactate dehydrogenase. *Proteins-Structure Function and Genetics* **2001,** *43*, 175-185.

11. Yao, Y. H.; Wang, H. T.; Li, B. G. LDH5 overexpression is associated with poor survival in patients with solid tumors: A meta-analysis. *Tumor Biology* **2014,** *35*, 6973-6981.

12. Yao, F.; Zhao, T. J.; Zhong, C. X.; Zhu, J.; Zhao, H. LDHA is necessary for the tumorigenicity of esophageal squamous cell carcinoma. *Tumor Biology* **2013,** *34*, 25-31.

13. Shi, M.; Cui, J.; Du, J.; Wei, D.; Jia, Z.; Zhang, J.; Zhu, Z.; Gao, Y.; Xie, K. A novel KLF4/LDHA signaling pathway regulates aerobic glycolysis in and progression of pancreatic cancer. *Clin Cancer Res* **2014,** *20*, 4370-4380.

14. Girgis, H.; Masui, O.; White, N. M. A.; Scorilas, A.; Rotondo, F.; Seivwright, A.; Gabril, M.; Filter, E. R.; Girgis, A. H. A.; Bjarnason, G. A.; Jewett, M. A. S.; Evans, A.; Al-Haddad, S.; Siu, K. W. M.; Yousef, G. M. Lactate dehydrogenase A is a potential prognostic marker in clear cell renal cell carcinoma. *Molecular Cancer* **2014,** *13*, 101.

15. Koukourakis, M. I.; Giatromanolaki, A.; Sivridis, E.; Bougioukas, G.; Didilis, V.; Gatter, K. C.; Harris, A. L.; Grp, T. A. R. Lactate dehydrogenase-5 (LDH-5) overexpression in non-small-cell lung cancer tissues is linked to tumour hypoxia, angiogenic factor production and poor prognosis. *Brit J Cancer* **2003,** *89*, 877-885.

16. Kolev, Y.; Uetake, H.; Takagi, Y.; Sugihara, K. Lactate dehydrogenase-5 (LDH-5) expression in human gastric cancer: Association with hypoxia-inducible factor (HIF-1alpha) pathway, angiogenic factors production and poor prognosis. *Ann Surg Oncol* **2008,** *15*, 2336-2344.

17. Lu, R. Q.; Jiang, M. L.; Chen, Z. J.; Xu, X. F.; Hu, H. F.; Zhao, X. M.; Gao, X.; Guo, L. Lactate dehydrogenase 5 expression in non-hodgkin lymphoma is associated with the induced hypoxia regulated protein and poor prognosis. *Plos One* **2013,** *8*, e74853.

18. Dong, T.; Liu, Z.; Xuan, Q.; Wang, Z.; Ma, W.; Zhang, Q. Tumor LDH-A expression and serum LDH status are two metabolic predictors for triple negative breast cancer brain metastasis. *Sci Rep* **2017,** *7*, 6069.

19. Valvona, C. J.; Fillmore, H. L.; Nunn, P. B.; Pilkington, G. J. The regulation and function of lactate dehydrogenase A: Therapeutic potential in brain tumor. *Brain Pathology* **2016,** *26*, 3-17.

20. Koukourakis, M. I.; Giatromanolaki, A.; Panteliadou, M.; Pouliliou, S. E.; Chondrou, P. S.; Mavropoulou, S.; Sivridis, E. Lactate dehydrogenase 5 isoenzyme overexpression defines resistance of prostate cancer to radiotherapy. *Br J Cancer* **2014,** *110*, 2217-2223.

21. Koukourakis, M. I.; Giatromanolaki, A.; Sivridis, E.; Gatter, K. C.; Trarbach, T.; Folprecht, G.; Shi, M. M.; Lebwohl, D.; Jalava, T.; Laurent, D.; Meinhardt, G.; Harris, A. L. Prognostic and predictive role of lactate dehydrogenase 5 expression in colorectal cancer patients treated with PTK787/ZK 222584 (Vatalanib) antiangiogenic therapy. *Clin Cancer Res* **2011,** *17*, 4892-4900.

22. Le, A.; Cooper, C. R.; Gouw, A. M.; Dinavahi, R.; Maitra, A.; Deck, L. M.; Royer, R. E.; Jagt, D. L. V.; Semenza, G. L.; Dang, C. V. Inhibition of lactate dehydrogenase A induces oxidative stress and inhibits tumor progression. *Proceedings of the National Academy of Sciences of the United States of America* **2010,** *107*, 2037-2042.

23. Boudreau, A.; Purkey, H. E.; Hitz, A.; Robarge, K.; Peterson, D.; Labadie, S.; Kwong, M.; Hong, R.; Gao, M.; Del Nagro, C.; Pusapati, R.; Ma, S. G.; Salphati, L.; Pang, J.; Zhou, A. H.; Lai, T.; Li, Y. J.; Chen, Z. G.; Wei, B. Q.; Yen, I.; Sideris, S.; McCleland, M.; Firestein, R.; Corson, L.; Vanderbilt, A.; Williams, S.; Daemen, A.; Belvin, M.; Eigenbrot, C.; Jackson, P. K.; Malek, S.; Hatzivassiliou, G.; Sampath, D.; Evangelista, M.; O'Brien, T. Metabolic plasticity underpins innate and acquired resistance to LDHA inhibition. *Nature Chemical Biology* **2016,** *12*, 779-786.

24. Fantin, V. R.; St-Pierre, J.; Leder, P. Attenuation of LDH-A expression uncovers a link between glycolysis, mitochondrial physiology, and tumor maintenance. *Cancer Cell* **2006,** *9*, 425-434.

25. Sheng, S. L.; Liu, J. J.; Dai, Y. H.; Sun, X. G.; Xiong, X. P.; Huang, G. Knockdown of lactate dehydrogenase A suppresses tumor growth and metastasis of human hepatocellular carcinoma. *Febs J* **2012,** *279*, 3898-3910.

26. Wang, Z. Y.; Loo, T. Y.; Shen, J. G.; Wang, N.; Wang, D. M.; Yang, D. P.; Mo, S. L.; Guan, X. Y.; Chen, J. P. LDH-A silencing suppresses breast cancer tumorigenicity through

induction of oxidative stress mediated mitochondrial pathway apoptosis. *Breast Cancer Res Treat* **2012,** *131*, 791-800.

27. Yip, S. S.; Zhou, M.; Joly, J.; Snedecor, B.; Shen, A.; Crawford, Y. Complete knockout of the lactate dehydrogenase A gene is lethal in pyruvate dehydrogenase kinase 1, 2, 3 down-regulated CHO cells. *Mol Biotechnol* **2014,** *56*, 833-838.

28. Kanno, T.; Sudo, K.; Maekawa, M.; Nishimura, Y.; Ukita, M.; Fukutake, K. Lactate-dehydrogenase M-subunit deficiency - a new type of hereditary exertional myopathy. *Clinica Chimica Acta* **1988,** *173*, 89-98.

29. Feng, Y.; Xiong, Y.; Qiao, T.; Li, X.; Jia, L.; Han, Y. Lactate dehydrogenase A: A key player in carcinogenesis and potential target in cancer therapy. *Cancer Med* **2018,** *7*, 6124-6136.

30. Rani, R.; Kumar, V. Recent update on human lactate dehydrogenase enzyme 5 (hLDH5) inhibitors: A promising approach for cancer chemotherapy. *J Med Chem* **2016,** *59*, 487-496.

31. Yang, Y.; Su, D.; Zhao, L.; Zhang, D.; Xu, J.; Wan, J.; Fan, S.; Chen, M. Different effects of LDH-A inhibition by oxamate in non-small cell lung cancer cells. *Oncotarget* **2014,** *5*, 11886-11896.

32. Fauber, B. P.; Dragovich, P. S.; Chen, J. H.; Corson, L. B.; Ding, C. Z.; Eigenbrot, C.; Giannetti, A. M.; Hunsaker, T.; Labadie, S.; Liu, Y. H.; Liu, Y. C.; Malek, S.; Peterson, D.; Pitts, K.; Sideris, S.; Ultsch, M.; VanderPorten, E.; Wang, J.; Wei, B. Q.; Yen, I.; Yue, Q. Identification of 2-amino-5-aryl-pyrazines as inhibitors of human lactate dehydrogenase. *Bioorg Med Chem Lett* **2013,** *23*, 5533-5539.

33. Dragovich, P. S.; Fauber, B. P.; Corson, L. B.; Ding, C. Z.; Eigenbrot, C.; Ge, H. X.; Giannetti, A. M.; Hunsaker, T.; Labadie, S.; Liu, Y. C.; Malek, S.; Pan, B.; Peterson, D.; Pitts, K.; Purkey, H. E.; Sideris, S.; Ultsch, M.; VanderPorten, E.; Wei, B. Q.; Xu, Q.; Yen, I.; Yue, Q.; Zhang, H. H.; Zhang, X. Y. Identification of substituted 2-thio-6-oxo-1,6-

dihydropyrimidines as inhibitors of human lactate dehydrogenase. *Bioorg Med Chem Lett* **2013,** *23*, 3186-3194.

34. Purkey, H. E.; Robarge, K.; Chen, J.; Chen, Z.; Corson, L. B.; Ding, C. Z.; DiPasquale, A. G.; Dragovich, P. S.; Eigenbrot, C.; Evangelista, M.; Fauber, B. P.; Gao, Z.; Ge, H.; Hitz, A.; Ho, Q.; Labadie, S. S.; Lai, K. W.; Liu, W.; Liu, Y.; Li, C.; Ma, S.; Malek, S.; O'Brien, T.; Pang, J.; Peterson, D.; Salphati, L.; Sideris, S.; Ultsch, M.; Wei, B.; Yen, I.; Yue, Q.; Zhang, H.; Zhou, A. Cell active hydroxylactam inhibitors of human lactate dehydrogenase with oral bioavailability in mice. *ACS Med Chem Lett* **2016,** *7*, 896-901.

35. Rai, G.; Brimacombe, K. R.; Mott, B. T.; Urban, D. J.; Hu, X.; Yang, S. M.; Lee, T. D.; Cheff, D. M.; Kouznetsova, J.; Benavides, G. A.; Pohida, K.; Kuenstner, E. J.; Luci, D. K.; Lukacs, C. M.; Davies, D. R.; Dranow, D. M.; Zhu, H.; Sulikowski, G.; Moore, W. J.; Stott, G. M.; Flint, A. J.; Hall, M. D.; Darley-Usmar, V. M.; Neckers, L. M.; Dang, C. V.; Waterson, A. G.; Simeonov, A.; Jadhav, A.; Maloney, D. J. Discovery and optimization of potent, cell-active pyrazole-based inhibitors of lactate dehydrogenase (LDH). *J Med Chem* **2017,** *60*, 9184-9204.

36. Zhou, Y.; Tao, P. D.; Wang, M. G.; Xu, P.; Lu, W.; Lei, P.; You, Q. Y. Development of novel human lactate dehydrogenase A inhibitors: High-throughput screening, synthesis, and biological evaluations. *Eur J Med Chem* **2019,** *177*, 105-115.

37. Poli, G.; Granchi, C.; Aissaoui, M.; Minutolo, F.; Tuccinardi, T. Three-dimensional analysis of the interactions between hLDH5 and its inhibitors. *Molecules* **2017,** *22*, 2217.

38. Hermann, R.; Jaenicke, R.; Rudolph, R. Analysis of the reconstitution of oligomeric enzymes by cross-linking with glutaraldehyde - kinetics of reassociation of lactic-dehydrogenase. *Biochemistry* **1981,** *20*, 5195-5201.

39. Yuan, C.; Hu, H.; Xu, G. Single amino-acid substitution in the N-terminal arm altered the tetramer stability of rat muscle lactate dehydrogenase A. *Sci China C Life Sci* **2001,** *44*, 576-584.

40. Pelay-Gimeno, M.; Glas, A.; Koch, O.; Grossmann, T. N. Structure-based design of inhibitors of protein-protein interactions: Mimicking peptide binding epitopes. *Angew Chem Int Ed Engl* **2015,** *54*, 8896-8927.

41. Cunningham, A. D.; Qvit, N.; Mochly-Rosen, D. Peptides and peptidomimetics as regulators of protein-protein interactions. *Curr Opin Struc Biol* **2017,** *44*, 59-66.

42. Ran, X.; Gestwicki, J. E. Inhibitors of protein-protein interactions (PPIs): An analysis of scaffold choices and buried surface area. *Curr Opin Chem Biol* **2018,** *44*, 75-86.

43. Touti, F.; Gates, Z. P.; Bandyopadhyay, A.; Lautrette, G.; Pentelute, B. L. In-solution enrichment identifies peptide inhibitors of protein-protein interactions. *Nat Chem Biol* **2019,** *15*, 410-418.

44. Wang, C. K.; Craik, D. J. Designing macrocyclic disulfide-rich peptides for biotechnological applications. *Nat Chem Biol* **2018,** *14*, 417-427.

45. Wuo, M. G.; Arora, P. S. Engineered protein scaffolds as leads for synthetic inhibitors of protein-protein interactions. *Curr Opin Chem Biol* **2018,** *44*, 16-22.

46. Jauset, T.; Beaulieu, M. E. Bioactive cell penetrating peptides and proteins in cancer: A bright future ahead. *Curr Opin Pharmacol* **2019,** *47*, 133-140.

47. Craik, D. J.; Fairlie, D. P.; Liras, S.; Price, D. The future of peptide-based drugs. *Chemical Biology & Drug Design* **2013,** *81*, 136-147.

48. Dobeli, H.; Schoenenberger, G. A. Regulation of lactate dehydrogenase activity: Reversible and isoenzyme-specific inhibition of the tetramerization process by peptides. *Experientia* **1983,** *39*, 281-282.

49. Yamamoto, S.; Storey, K. B. Dissociation-association of lactate dehydrogenase isozymes: Influences on the formation of tetramers versus dimers of M4-LDH and H4-LDH. *Int J Biochem* **1988,** *20*, 1261-1265.

50. Zheng, Y. B.; Guo, S. Y.; Guo, Z.; Wang, X. C. Effects of N-terminal deletion mutation on rabbit muscle lactate dehydrogenase. *Biochemistry-Moscow* **2004,** *69*, 401-406.

51. Fan, J.; Hitosugi, T.; Chung, T. W.; Xie, J. X.; Ge, Q. Y.; Gu, T. L.; Polakiewicz, R. D.; Chen, G. Z.; Boggon, T. J.; Lonial, S.; Khuri, F. R.; Kang, S. M.; Chen, J. Tyrosine phosphorylation of lactate dehydrogenase A is important for NADH/NAD(+) redox homeostasis in cancer cells. *Molecular and Cellular Biology* **2011,** *31*, 4938-4950.

52. Jin, L.; Chun, J.; Pan, C.; Alesi, G. N.; Li, D.; Magliocca, K. R.; Kang, Y.; Chen, Z. G.; Shin, D. M.; Khuri, F. R.; Fan, J.; Kang, S. Phosphorylation-mediated activation of LDHA promotes cancer cell invasion and tumour metastasis. *Oncogene* **2017,** *36*, 3797-3806.

53. Jafary, F.; Ganjalikhany, M. R.; Moradi, A.; Hemati, M.; Jafari, S. Novel peptide inhibitors for lactate dehydrogenase A (LDHA): A survey to inhibit LDHA activity via disruption of protein-protein interaction. *Sci Rep* **2019,** *9*, 4686.

54. Tenenbaum-Bayer, H.; Levitzki, A. The refolding of lactate dehydrogenase subunits and their assembly to the functional tetramer. *Biochim Biophys Acta* **1976,** *445*, 261-279.

55. Dobeli, H.; Gillessen, D.; Lergier, W.; Van Dijk, A.; Schoenenberger, G. A. Inhibition of the reactivation of acid-dissociated lactate dehydrogenase isoenzymes by their aminoterminal CNBr fragments. *Peptides* **1987,** *8*, 773-778.

56. Das, R.; Qian, B.; Raman, S.; Vernon, R.; Thompson, J.; Bradley, P.; Khare, S.; Tyka, M. D.; Bhat, D.; Chivian, D.; Kim, D. E.; Sheffler, W. H.; Malmstrom, L.; Wollacott, A. M.; Wang, C.; Andre, I.; Baker, D. Structure prediction for CASP7 targets using extensive all-atom refinement with rosetta@home. *Proteins* **2007,** *69 Suppl 8*, 118-128.

57. Das, R.; Baker, D. Macromolecular modeling with rosetta. *Annu Rev Biochem* **2008,** *77*, 363-382.

58. Silva, P. I., Jr.; Daffre, S.; Bulet, P. Isolation and characterization of gomesin, an 18-residue cysteine-rich defense peptide from the spider Acanthoscurria gomesiana hemocytes with sequence similarities to horseshoe crab antimicrobial peptides of the tachyplesin family. *J Biol Chem* **2000,** *275*, 33464-33470.

59. Mandard, N.; Bulet, P.; Caille, A.; Daffre, S.; Vovelle, F. The solution structure of gomesin, an antimicrobial cysteine-rich peptide from the spider. *Eur J Biochem* **2002,** *269*, 1190-1198.

60. Henriques, S. T.; Lawrence, N.; Chaousis, S.; Ravipati, A. S.; Cheneval, O.; Benfield, A. H.; Elliott, A. G.; Kavanagh, A. M.; Cooper, M. A.; Chan, L. Y.; Huang, Y. H.; Craik, D. J. Redesigned spider peptide with improved antimicrobial and anticancer properties. *Acs Chemical Biology* **2017,** *12*, 2324-2334.

61. Benfield, A. H.; Defaus, S.; Lawrence, N.; Chaousis, S.; Condon, N.; Cheneval, O.; Huang, Y. H.; Chan, L. Y.; Andreu, D.; Craik, D. J.; Henriques, S. T. Cyclic gomesin, a stable redesigned spider peptide able to enter cancer cells. *Biochim Biophys Acta Biomembr* **2020,** *1863*, 183480.

62. Cheneval, O.; Schroeder, C. I.; Durek, T.; Walsh, P.; Huang, Y. H.; Liras, S.; Price, D. A.; Craik, D. J. Fmoc-based synthesis of disulfide-rich cyclic peptides. *Journal of Organic Chemistry* **2014,** *79*, 5538-5544.

63. Nakamura, T.; Furunaka, H.; Miyata, T.; Tokunaga, F.; Muta, T.; Iwanaga, S.; Niwa, M.; Takao, T.; Shimonishi, Y. Tachyplesin, a class of antimicrobial peptide from the hemocytes of the horseshoe crab (Tachypleus tridentatus). Isolation and chemical structure. *J Biol Chem* **1988,** *263*, 16709-16713.

64. Vernen, F.; Harvey, P. J.; Dias, S. A.; Veiga, A. S.; Huang, Y. H.; Craik, D. J.; Lawrence, N.; Troeira Henriques, S. Characterization of tachyplesin peptides and their cyclized analogues to improve antimicrobial and anticancer properties. *Int J Mol Sci* **2019,** *20*, 4184.

65. Webb, B.; Sali, A. Comparative protein structure modeling using modeller. *Curr Protoc Protein Sci* **2016,** *54*, 5.6.1-5.6.37.

66. Thabault, L.; Brisson, L.; Brustenga, C.; Gache, S. A. M.; Prevost, J. R. C.; Kozlova, A.; Spillier, Q.; Liberelle, M.; Benyahia, Z.; Messens, J.; Copetti, T.; Sonveaux, P.; Frederick, R. Interrogating the lactate dehydrogenase tetramerization site using (stapled) peptides. *J Med Chem* **2020,** *63*, 4628-4643.

67. Conway, P.; Tyka, M. D.; DiMaio, F.; Konerding, D. E.; Baker, D. Relaxation of backbone bond geometry improves protein energy landscape modeling. *Protein Sci* **2014,** *23*, 47-55.

68. Kuhlman, B.; Dantas, G.; Ireton, G. C.; Varani, G.; Stoddard, B. L.; Baker, D. Design of a novel globular protein fold with atomic-level accuracy. *Science* **2003,** *302*, 1364-1368.

69. Henriques, S. T.; Huang, Y. H.; Chaousis, S.; Sani, M. A.; Poth, A. G.; Separovic, F.; Craik, D. J. The prototypic cyclotide kalata B1 has a unique mechanism of entering cells. *Chemistry & Biology* **2015,** *22*, 1087-1097.

Table of contents graphic